International Journal of Hydrogen Energy 178 (2025) 151655

Contents lists available at ScienceDirect

International Journal of Hydrogen Energy

journal homepage: www.elsevier.com/locate/he

Experimental study of H_2 injection strategies in a HD engine: Comparison of PFI and LPDI

Jinlin Han [a,b,*], Erik Doosje [a], Xander Seykens [a,b], L.M.T. Somers [b]

[a] TNO Powertrain, Helmond, Netherlands
[b] Department of mechanical engineering, Eindhoven University of Technology, Netherlands

ARTICLE INFO

Handling Editor: Dr M Mahdi Najafpour

Keywords:
H2
HD engine
Injection strategy
NOx
Efficiency

ABSTRACT

Stringent CO_2 reduction targets and tightening emission regulations have intensified interest in hydrogen internal combustion engines (H2ICEs) as a clean and robust solution for the heavy-duty (HD) sector. This study experimentally compares port fuel injection (PFI), early low-pressure direct injection (LPDI), and late LPDI strategies on a single-cylinder HD H2ICE under steady-state medium and high loads. The injection timing and fuel pressure are varied to study the overall influences on a single-cylinder heavy-duty H2ICE. PFI and early LPDI deliver high charge homogeneity but reduced volumetric efficiency compared to late LPDI. At medium load, all three strategies achieve ~41 % gross indicated thermal efficiency (gITE). Increasing LPDI pressure from 12.8 to 20 bar enhances mixture uniformity, cutting $BSNO_x$ emissions by up to 75 %. At high load, early LPDI reaches 41.7 % gITE with low NO_x (0.72 g/kWh), while late LPDI benefits from reduced heat transfer loss and compression work, achieving 42.4 % gITE. However, late injection also increases $BSNO_x$ (9.3 g/kWh), unburnt H_2 (435 ppm), and pressure rise rate (19.7 bar/°CA). These results highlight LPDI's potential for high efficiency, with injection timing and pressure as key levers to balance emissions and performance.

Abbreviations

aTDC	After top dead center	HD	Heavy-duty
BD	Burn duration	H2ICE	Hydrogen internal combustion engine
BDC	Bottom dead center	H_2	Hydrogen
BMEP	Brake mean effective pressure	ICE	Internal combustion engine
BSNOx	Indicated specific nitro-oxide	IMEP	Indicated mean effective pressure
BTE	Brake thermal efficiency	LPDI	Low pressure direct injection
°CA	Crank angle	ITE	Indicated thermal efficiency
CR	Compression ratio	NOx	Nitrogen oxides
DI	Direction injection	OEM	Original equipment manufacture
EGR	Exhaust gas recirculation	PFI	Port fuel injection
EOI	End of injection	PRR	Pressure rise rate
EU	European union	RPM	Rotation per minute
gITE	Gross indicated thermal efficiency	SOI	Start of injection
GHG	Greenhouse gas		

1. Introduction

The European Climate Law, as part of the European Green Deal, aims to transition Europe's economy and society toward climate neutrality by 2050. An intermediate target has been established to reduce net greenhouse gas (GHG) emissions by at least 55 % by 2030 [1]. The transportation sector plays a significant role in this context, accounting for 32 % of carbon dioxide (CO_2) emissions in Europe [2]. Within this sector, light-duty vehicles contribute approximately 15 % of EU CO_2 emissions, while heavy-duty vehicles are responsible for over a quarter of CO_2 emissions from road transport, constituting about 6 % of the total GHG emissions in the EU [3]. To address these challenges, the European Parliament has adopted stringent regulations, mandating a 90 % reduction in CO_2 emissions from new trucks by 2040. Specifically, new trucks are required to reduce CO_2 emissions by 43 % by 2030 (compared to 2019 levels), 64 % by 2035, and 90 % by 2040. For city buses, the transition is even more aggressive, with 90 % of sales mandated to be zero-emission by 2030 and a complete phase-out of fossil-fueled buses by 2035 [4]. Additionally, the introduction of the stringent Euro 7 emission standards imposes further challenges on original equipment manufacturers (OEMs) worldwide. These regulatory measures present

* Corresponding author. TNO Powertrain, Helmond, Netherlands.
E-mail addresses: j.han.1@tue.nl, jinlin.han@tno.nl (J. Han).

https://doi.org/10.1016/j.ijhydene.2025.151655
Received 11 July 2025; Received in revised form 15 September 2025; Accepted 18 September 2025
Available online 24 September 2025

significant obstacles but also serve as critical drivers for innovation in the transportation sector.

Hydrogen, as a promising energy carrier, has gained significant attention due to its high energy density (H_2:119.7 MJ/kg vs CH_4:50 MJ/kg [5]), sustainability, and zero-carbon emissions. These attributes position hydrogen as a renewable and carbon-neutral alternative fuel, capable of leveraging advancements in state-of-the-art internal combustion engine (ICE) technology. Hydrogen-fueled internal combustion engines (H2ICEs) offer a practical pathway toward carbon-neutral transport by leveraging existing engine platforms while eliminating CO_2 emissions at the tailpipe [6]. The hydrogen internal combustion engine (H2ICE) offers several distinct advantages, including established engine research and development, and a well-developed engine supply chain. These strengths make H2ICE a potential technical solution for applications such as off-road sectors (e.g. agriculture, construction, and power generation), long-haul heavy-duty road transportation, and marine shipping [7]. The aforementioned heavy equipment either faces challenges in being battery-powered or suffers from a lack of accessible electricity. Moreover, the zero-carbon emissions of H2ICE provide a compelling advantage over alternative technological pathways such as fuel cells, particularly when considering factors such as affordability, minimized need for substantial infrastructure investment, and the ease of retrofitting existing engines (PFI, for example). These benefits position H2ICE as both a near-term and long-term solution for achieving carbon neutrality, especially in sectors where electrification may not be practical or economically feasible [8]. Compared with conventional fossil fuels, hydrogen enables high indicated efficiency due to its wide flammability range and fast flame speed, yet poses unique challenges related to backfire, pre-ignition, and NO_x formation [9]. To realize high efficiency with ultra-low emissions, H2ICE requires tailored design changes including optimized injection strategies, improved mixture preparation, and advanced aftertreatment solutions [10]. Recent studies have highlighted both the opportunities and technical hurdles of deploying H2ICEs in heavy-duty and aviation sectors, emphasizing the need for systematic experimental research on injection strategies to balance efficiency [11,12].

It should be noted that hydrogen presents a low volumetric energy density compared to natural gas (H_2 10.8 MJ/m^3 vs. CH_4 35.8 MJ/m^3 [5]). Consequently, high volumetric flow rates are necessary to meet the demand of high engine load ranges. Based on how hydrogen is introduced into the engine and the mixture formation types, Fig. 1 presents an overview of potential hydrogen combustion concepts intended for HD engines. Among them, three major H2ICE concepts are taken as the most mature solutions for vehicle application: port fuel injection (PFI), low-pressure direct injection (LPDI), and high-pressure direct injection (HPDI). The mainstream HPDI technology requires highly-reactive fuel (for example: diesel) to ignite prior to the direct injected H_2 (H_2 pressure: 200–300 bar) [14], which introduces additional CO_2 emissions. Seykens et al. reported that HPDI achieves a net indicated thermal efficiency (nITE) of 47–48 % with engine-out NOx emissions in the range of 6–7 g/kWh at 24 bar brake mean effective pressure (BMEP). This performance is achieved without the need for new or updated hardware, utilizing a base engine platform that closely resembles current diesel engine designs. In contrast, Port Fuel Injection (PFI) systems require additional measures such as water injection, compression reduction, and high boost pressures exceeding 4 bar [15]. Further investigation is necessary to determine whether HPDI technology can meet the Vecto CO_2 standard. As this study primarily compared PFI and LPDI systems, the discussion of HPDI falls outside the scope of this work and will not be addressed further.

PFI benefits from a high degree of homogeneity, resulting in less high temperature zones and thermal NOx formation is close to zero at sufficiently lean mixtures (lambda = 2.5 [16]). Yet, studies have shown that PFI in hydrogen engines results in a notable reduction in volumetric efficiency as hydrogen occupies approximately 30 % of the intake volume, reducing power density compared to DI systems [17,18]). Despite this limitation, advanced turbocharging strategies can compensate for the loss. For instance, Lai et al. optimized turbo-matching in a 5.13L PFI H2ICE to achieve 128.9 kW of maximum power and 662.6 Nm of torque—an improvement of 38.7 % and 7.7 %, respectively, compared to the original configuration [19]. The maximum reduced mass flow of the selected turbine is extended to 0.0156 (kg/s)*K^0.5/kPa. Additionally, simulation studies reveal that PFI H2ICE requires 50 % higher mass flow and 90 % higher boost pressure than conventional turbocharged gasoline engines. These demands require two-stage boosting systems with variable geometry turbines at the high-pressure stage [20]. Practical implementation by Frigo et al. demonstrated that a converted H2ICE (retrofitted from natural gas engine) retained high efficiency (>39 %) and low NOx emissions (<200 ppm) under PFI operation at a lambda 2.5, albeit with a 10 % loss in torque and power compared to its methane-fueled baseline [21]. DI systems mitigate the volumetric efficiency issues of PFI by injecting hydrogen directly into the combustion chamber, enabling higher power density and improved thermal efficiency. Experiments on a light-duty single-cylinder H2ICE (displacement: 0.4L, CR:11.3) by Mohamed et al. showed that LPDI achieved 2 % higher indicated thermal efficiency (ITE) than PFI due to reduced pumping losses and hydrogen slip in the exhaust. Furthermore, LPDI required lower boost pressures, reducing pumping loss and demand on the boosting system [22]. Both concepts demonstrate near-zero NOx emissions at lambda 2.5–3.7. In addition, positive valve overlap can be used on LPDI to enhance the scavenging effects. This is also confirmed by Silveria et al. that valve overlap should be eliminated or minimized for PFI H2ICE to prevent backfire in the intake manifold [23]. They highlighted that load is largely constrained by the compressor power. Furthermore, knock was detected at lambda <1.8, and combustion became unstable at lambda>3. The low density and high diffusivity of hydrogen present significant challenges in achieving an optimal mixture adjustment [24]. It is found that the deflector structure of the LPDI H_2 injector determines the first movement path of the hydrogen. Simulation results show that a single hole 12° tilted upwards forms a concentrated region and reaches a 42.9 % indicated thermal efficiency. Although both injection timing and pressure affect the interaction between the

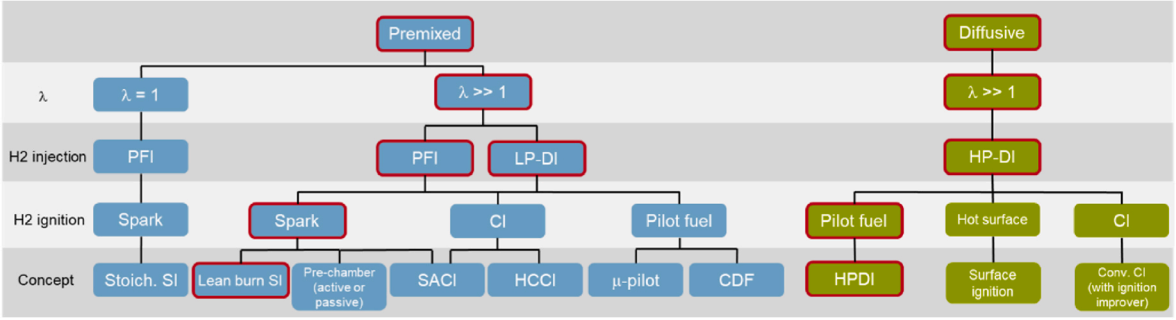

Fig. 1. H2ICE concepts and related fueling and injection systems [13]. Reprinted with permission from [Bekdemir, C., SAE Technical Paper 2022-01-0472, 2022].

hydrogen jet and the cylinder flow field, and thus alter the distribution of mixture at ignition timing [24], injection timing appears to be more influential in improving engine performance. Up to 44.05 % indicated thermal efficiency is achieved at injection timing of −100 crank angle degree after top dead center (^{o}CA aTDC). Furthermore, compared with the original single injection, the delayed single injection and two-stage injection result in higher stratification and up to 44.7 % indicated thermal efficiency is achieved at the expense of much higher NOx emissions.

The aforementioned research on PFI H2ICE has been primarily conducted on passenger vehicle engines or light-duty engines. Similarly, the development of LPDI engines has also focused on these categories of engines. Researchers have extensively examined various direct injection (DI) systems to enhance the performance, efficiency, and emissions profile of H2ICE. Lee et al. compared the H_2/air mixture formation under homogeneous mode (injection: 158^{o}CA aTDC, lambda 1) lean-homogeneous mode (injection: 158^{o}CA aTDC, lambda1.7/1.75) and lean-stratified mode (injection: 26/-44^{o}CA aTDC lambda 2.3/1.95) on a single cylinder LPDI H2ICE platform (CR:12 displacement: 0.5L) [25]. It is shown that lean stratified combustion yields the highest ITE of 34.09 % because of lower exhaust loss and heat transfer loss. Yet due to the local rich H_2 rich mixture also leads to the higher engine-out NOx emissions (low load:6.68g/kWh, high load: 10.84 g/kWh). In contrast, lean homogeneous mode produced the lowest NOx emissions (low load: 2.21 g/kWh, high load: 1.59 g/kWh). Among all three combustion modes, the homogeneous mode produces the highest engine-out NOx emissions because of stochiometric combustion (lambda 1) and lowest ITE (20 % throttling valve, pumping loss, and heat loss). Molina et al. investigated an outwardly opening poppet valve DI system for hydrogen injection in a 0.45L single-cylinder engine (compression ratio: 10.7) designed for light-duty applications [26]. A PFI system was also employed for comparative analysis under the following test conditions. Engine tests were conducted at 1500 rpm, with indicated mean effective pressures (IMEP) of 4 and 6 bar, lambda values ranging from 2.2 to 3.2, and start of injection (SOI) timings between −130 and −85 crank angle (^{o}CA). It was found that LPDI requires less boost pressure than PFI. The LPDI system achieved a 0.6 %−1.1 % improvement in gross indicated efficiency (gITE) relative to the PFI system under identical operating conditions. The gITE exhibited an increasing trend with higher lambda values, peaking at 41.2 % for $\lambda = 3.2$ at IMEP = 4 bar and 41.5 % for $\lambda = 3$ at IMEP = 6 bar. However, these efficiency gains were accompanied by diminished combustion efficiency for both LPDI and PFI systems. Delayed SOI timings reduced compression work by 7.6 % and 3.9 % at 4 and 6 bar IMEP respectively, which corresponded to a 3.1 %–3.2 % decrease in fuel consumption. Nevertheless, shorter mixing times at late SOI led to charge stratification and locally rich hydrogen combustion, contributing to increased NOx emissions. The trends and levels of NOx emissions were found to be comparable between LPDI and PFI systems, indicating limited differentiation in emission performance under the test conditions. Thawko et al. compared the combustion performance and emissions characteristics of hydrogen, methane, and reformate gas (CO2+H2) in a LPDI single-cylinder engine (displacement: 0.37L, compression ratio: 15.5) [27]. The engine was operated at a constant speed of 2700 rpm with IMEP values ranging from 4 to 5.5 bar. Hydrogen combustion demonstrated the shortest burn duration and the highest ITE among the three tested fuels, attributed to its unthrottled lean combustion properties. Hydrogen exhibited lower NOx emissions than methane up to 4.9 bar IMEP, despite its higher rate of heat release. However, gITE decreased at late injection timings, likely due to impaired hydrogen-air mixing. It should be noted that hydrogen combustion yields a higher particulate number than methane combustion at 5.5 bar IMEP, which is likely associated with hydrogen's shorter quenching distance and the consequent enhancement of lubricant oil evaporation.

In addition to experimental studies, simulation-based investigations of H2ICE are increasingly prevalent due to their cost-effectiveness and ability to provide deeper insights into complex in-cylinder phenomena. These simulations allow for detailed examination of combustion processes, emissions formation, and optimization strategies for H2ICE systems. For instance, Maio et al. utilized a 3D Reynolds-Averaged Navier-Stokes (RANS) approach combined with the Extended Coherent Flame Model (ECFM) to simulate critical aspects of H2ICE operation, including spark ignition, flame propagation, auto-ignition, and NOx formation [28]. Their model effectively captured knocking and NOx trends observed in experimental conditions. For PFI scenarios, slight re-calibration of the turbulent strain source term was necessary to account for richer operating conditions due to the absence of preferential diffusion effects in the model. Gammaidoni et al. conducted numerical studies on a 0.5L optical single-cylinder engine (CR: 9) to compare PFI and DI systems under various injection timings and lambda conditions (up to lambda = 3.5) [29]. The study revealed that PFI maintained high combustion efficiency up to lambda = 3, after which it dropped significantly (e.g., 70 % combustion efficiency at lambda = 3.5). Injection timing showed minimal influence on combustion efficiency for LPDI at lambda = 2, though earlier injection timing improved H_2/air mixing. However, as lambda increased, combustion efficiency decreased across both PFI and LPDI, with late injection timing exacerbating these effects by slowing turbulent combustion. Recent research highlights the benefits of advanced injection timing and extended injection duration in DI systems, which promote mixture homogeneity, enhance flame propagation, and improve combustion efficiency [30]. However, when injection occurs after the intake valve opens, hydrogen backflow into the intake manifold can occur, depending on the timing and duration of injection. Musy et al. employed ANSYS Forte to simulate PFI and DI configurations in a naturally aspirated Volkswagen engine (displacement:1.4 L, CR:10.5) [31]. The DI configuration showed superior performance, delivering: 39.5 % increase in brake power, 30.6 % improvement in volumetric efficiency and 37.6 % reduction in NOx emissions compared to PFI. The reduction in NOx emissions was attributed to the stratified combustion and lower peak temperatures associated with DI.

Moreover, it is essential that the H_2 fuel flow is operated under choked conditions (i.e., sonic flow at Mach number = 1), as this ensures that the flow rate is governed solely by the injection duration, fuel pressure, and needle lift. For hydrogen, the critical pressure ratio is ~0.53 at a polytropic coefficient of ~1.4, indicating fuel pressure needs to be about 1.89 times the in-cylinder pressure [32]. In addition, hydrogen presents a low volumetric energy density compared to natural gas (10.8 MJ/m^3 vs 35.8 MJ/m^3 [33]), therefore high volumetric flow rates are necessitated to meet demand at high engine load range. This consideration is particularly critical for LPDI systems, where H_2 fuel pressure is limited to 40 bar, as specified by current mainstream injector manufacturers [33]. The low fuel pressure poses challenges to achieve choked flow during the late compression stroke due to the high in-cylinder pressure at this stage. The choked flow is more practical to realize for PFI system, where the downstream pressure corresponds to the boost pressure and thereby alleviating constraints of fuel pressure.

The findings from prior studies demonstrate the potential of PFI and LPDI on H2ICE to achieve high efficiency and low emissions from light-duty applications or passenger vehicles, with a notable lack of research on heavy-duty applications. The overall performance of H2ICE is significantly influenced by injection strategies and the specific requirements of the target application. Notably, both experimental and simulation studies have reported inconsistent results regarding the advantages of LPDI and PFI systems. And the comparison of PFI and LPDI have been conducted on different engine platforms. This study addresses these gaps by directly comparing PFI and LPDI systems using the single-cylinder HD H_2 engine. It has to be noted that most DI H2 injection starts after the intake valve closes, which reduces the risk of backfire. Still, backfire is one of the abnormal phenomena that needs to be reduced for PFI. This can be largely prevented by selecting a dedicated injection window. In this study, PFI H_2 injection was initiated only after a portion

of hydrogen-free fresh air had been inducted into the cylinder, which not only reduces the likelihood of pre-ignition but also provides an opportunity for dilution of the fresh charge with residual combustion gases from the previous cycle. To achieve a hydrogen-free mixture near the intake valve for the next cycle, the PFI injection window is terminated well before intake closing. This strategy further minimizes the potential for hot residual gases to come into direct contact with the injected hydrogen. LPDI is classified based on the SOI regimes into two categories: early LPDI (SOI between −300 and −200 °CA aTDC, before intake valve closes) and late LPDI (SOI between −150 and −90 °CA aTDC, after intake valve closes). These different injection regimes inevitably result in variations in charge homogeneity and stratification, which subsequently affect engine performance and emission characteristics. Guided by these research questions, this work also investigates the effects of fuel pressure and injection timing for both PFI and LPDI at both medium and high loads.

2. Experimental setup and approach

In this study, a single-cylinder research H_2 engine (spark ignition) platform was developed, targeting Euro 7 HD truck application. This single-cylinder HD engine has a compression ratio of 10.5 and a rated power of 60 kW. As illustrated in the schematic configuration in Fig. 2, the engine is equipped with a low-pressure direct injection (LPDI) system. Additionally, a port fuel injection (PFI, injector supplied by Nikki) system is also installed in the intake manifold. The LPDI hydrogen injector (supplied by Bosch) is capable of delivering gas at pressures up to 40 bar. The test rig was connected to an external air compressor to achieve the desired inlet boosting pressure. The hydrogen fuel used was 99.99% pure and supplied from a hydrogen storage tube trailer (240 kg of hydrogen per trailer) located adjacent to the test facility. This enables continuous testing of the heavy-duty engine. The engine cylinder was mounted with a Kistler 6054 in-cylinder pressure sensor. Since piezoelectric sensors are drift-sensitive, the intake manifold pressure was used to correct the drift of each individual cycle by equating the pressures at bottom dead center (BDC) of the intake stroke. The pressure signal was recorded at 0.1 °CA intervals using an AVL XION. Raw engine-out emissions were measured using a Horiba MEXA-ONE analyzer. Unburnt H_2 is detected by the Horiba system using mass spectrometry, which is designed to measure concentrations of hydrogen in exhaust gases accurately and quickly. Each measurement consisted of 100 cycles, collected by the data acquisition system, while the emission measurements were averaged over 30 s during the test. Throughout the tests, the engine speed was maintained at a constant 1000 rpm, and the brake mean effective pressure (BMEP) was kept constant. These speed-load points are representative of a typical cruise speed and medium (BMEP: 10 bar) and high load (BMEP: >19 bar) conditions on highways. Three injection strategies are specifically investigated: PFI, early LPDI (SOI between −300° and −200 °CA), and late LPDI (SOI between −150° and −90 °CA). The selection of the injection window preserves both the required injection duration to achieve the target load and the need to avoid backfire and pre-ignition. Note that the early LPDI is injected in the open valve period and the late LPDI is injected in the closed valve period. The investigation begins with varying the fuel pressure ranging from 4 to 10 bar for PFI and 13–30 bar for LPDI at medium load. This was followed by a SOI sweep at high load. All tests are performed with fixed inlet temperature of 44.5 ± 0.5 °C.

3. Data processing

In this work, the brake mean effective mean pressure (BMEP) is defined as follows:

$$BMEP = \frac{(2\cdot\pi\cdot M\cdot N/60)}{V_d} \quad \text{Equation 1}$$

Where M stands for the engine torque, N is engine speed in rpm, Vd represents the swept volume. And gross indicated thermal efficiency (gITE) is calculated by ratio between gross indicated work (W_g) and total energy input:

$$gITE = \frac{Wg}{Total} = \frac{\int_{-180}^{180} P\cdot dV}{\dot{m}_{fuel}\cdot LHV_{fuel}} \quad \text{Equation 2}$$

where $\dot{m}_{fuel}$ is fuel flow and LHV_{fuel} is the lower heating value of hydrogen, P is measured in-cylinder pressure (from −180 to 180°CA).

$$nIMEP = \frac{\int_{-360}^{360} P \times dV}{V_d} \quad \text{Equation 3}$$

For hydrogen combustion, the number of mole change after the combustion can differ significantly from the number of moles before

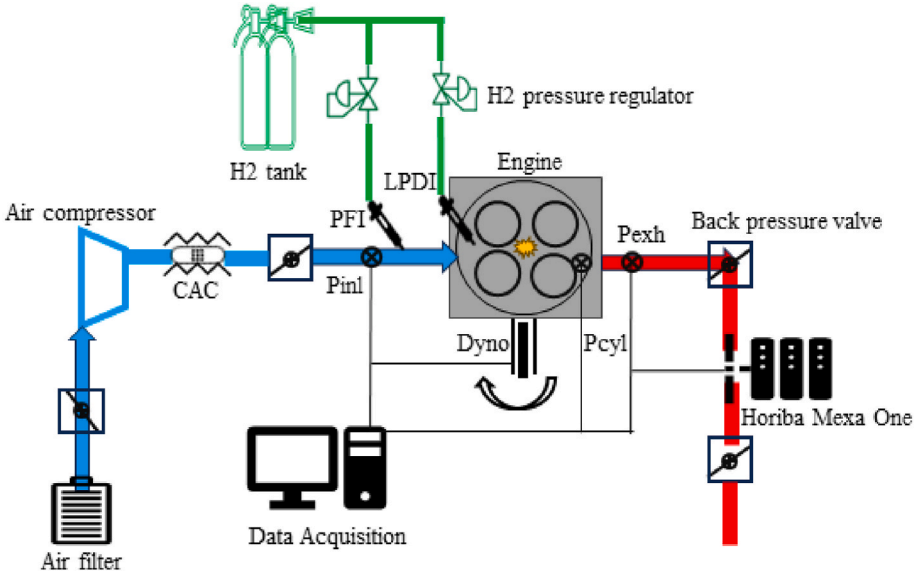

Fig. 2. Single-cylinder HD H2ICE test rig (CAC: compressor air cooling; Pinl: Inlet pressure; Pexh: exhaust pressure).

combustion, which is not the case for hydrocarbon-based fuel combustion. This distinction necessitates a tailored approach to heat release analysis, ensuring accurate assessment of the combustion process. In this work, the rate of heat release (ROHR) is determined according to:

$$ROHR = \frac{\gamma}{\gamma-1}P\frac{\partial V}{\partial \theta} + \frac{1}{\gamma-1}V\frac{\partial p}{\partial \theta} - \frac{1}{\gamma-1}PV\frac{1}{n}\frac{\partial n}{\partial \theta} \quad \text{Equation 4}$$

where $\frac{\partial V}{\partial \theta}$ is the volume change of the cylinder. The rate of mole during combustion is represented by $\frac{\partial n}{\partial \theta}$. The derivative of cylinder pressure, termed pressure rise rate (PRR), is denoted $\frac{\partial p}{\partial \theta}$.

ROHR is integrated to determine the cumulative heat released (HR). The combustion phasing parameters CA10, CA50 and CA90 are determined from 10, 50 and 90 % of the HR, respectively. Burn duration (BD) is the crank angle interval between CA10 and CA90, i.e. BD=CA90-CA10. These are taken from the HR with a heat loss correction using correlations (Woschni-type).

In this work, both abnormal combustion phenomena such as pre-ignition (PI) and general stability aspects such as the occurence of combustion instabilities are considered. Specifically, the coefficient of variance of nIMEP is used as an indicator of stability, defined according to Equation (5).

$$COVnIMEP = \frac{std(nIMEP)}{mean(nIMEP)} \cdot 100\% \quad \text{Equation 5}$$

Both the standard deviation (std) and mean are calculated over 100 cycles. Pre-ignition is a major challenge for H2ICE. It occurs when the hydrogen/air mixture ignites before the intended spark timing, resulting in uncontrolled combustion [34]. This advanced combustion phasing, causing higher pressure and temperature levels, can lead to knock when the unburnt hydrogen/air mixture auto-ignites before the flame front reaches it. Knocking combustion generates pressure waves that travel through the combustion chamber, potentially damaging engine components and impairing engine performance. Therefore, minimizing or eliminating uncontrolled combustion is crucial to protect engine hardware and maintain optimal performance. In this work, PI is defined as PI = spark timing-CA5, where positive values indicate that 5 % of the HR occurs before the sparking timing. The PI ratio is essentially the ratio of the number of PI cycles to the total recorded cycles in each measurement.

4. Uncertainty analysis

To reduce the influence of random errors such as cycle-to-cycle variations and high-frequency noise, all experimentally acquired data were processed per cycle and averaged over multiple consecutive engine cycles during post-processing. This statistical averaging significantly minimizes the random (Type A) uncertainty. However, systematic (Type B) uncertainties—originating from sources such as sensor calibration errors, pressure offset, full-scale (FS) error, and crank angle misalignment—remain present and must be addressed through uncertainty analysis. In this study, an error propagation method is applied to estimate the combined measurement uncertainty in the gross indicated thermal efficiency (gITE). The relative uncertainty in gITE, denoted as μgITE, is calculated by considering the major contributing sources:

$$\left(\frac{\mu gITE}{gITE}\right)^2 = \left(\frac{\mu Wg}{Wg}\right)^2 + \left(\frac{\mu \dot{m}_{fuel}}{\dot{m}_{fuel}}\right)^2 + \left(\frac{\mu LHV_{fuel}}{LHV_{fuel}}\right)^2 \quad \text{Equation 6}$$

Indicated work uncertainty μWg is load dependent, based on the pressure sensor's ±1 % FS accuracy and a crank angle resolution of 0.1°CA. Fuel mass flow rate uncertainty: $\mu\,\dot{m}_{fuel} \approx 0.25$ %, derived from the accuracy specification of the Coriolis flow meter. Fuel lower heating value uncertainty: μLHV ≈0.1 %, reflecting the certified 99.9 % purity of bottled hydrogen. The combined relative uncertainty in gITE is then computed using the root-sum-square (RSS) method, assuming the error sources are uncorrelated. The uncertainties of used apparatus in this work are summarized in Table 1.

5. Effects of fuel pressure at medium load

This section focuses on the influences of fuel pressure on PFI and LPDI. Table 2 displays the operating conditions for three injection strategies. The engine was operated in a steady-state condition at medium load (10 bar BMEP, 1000 RPM) with a fixed CA50, while the fuel pressure was varied. For both LPDI and PFI, the spark timing was adjusted to maintain CA50 at approximately 8 °CA aTDC, thereby compensating for the effects of fuel pressure and timing variations. This choice of CA50 represents a trade-off between avoiding knock and pre-ignition while ensuring high combustion efficiency. As a result, both CA10 and the burn duration (CA90–CA10) remained stable across the investigated fuel pressures, as illustrated in Fig. 3. To achieve a similar CA50, spark timing of PFI must be earlier than that of LPDI, likely due to an overall leaner H_2/air mixture. Interestingly, the late LPDI cases (SOI: 130/-140/-150 ^{o}CA) exhibit shorter burn durations (CA90-CA10) compared to PFI. This is attributed to increased charge stratification due to late injection timing, which accelerates the burn rate.

Fig. 4 compares the cylinder pressure and aROHR profiles of both PFI (−320 ^{o}CA aTDC) and early LPDI (−260 ^{o}CA aTDC) at same CA50. Intriguingly, PFI and LPDI show similar heat release processes despite the fuel pressure and timing differences. In this case, LPDI injection timing is −260 ^{o}CA aTDC during the intake stroke, and the mixing time for H_2 and air is apparently long enough to reach a similar charge homogeneity as PFI. Table 3 highlights the key performance metrics of these two measurements. While the combustion phasing (CA50, burn duration) and PRR are similar for both PFI and LPDI, PFI achieves a marginally higher gITE (41.5 ± 0.8 %) compared to early LPDI (41.0 ± 0.8 %). Note that this should not be interpreted as a definitive efficiency advantage for PFI, as it lies within the estimated 2 % relative systematic uncertainty of the measurements. Fig. 5a shows the engine-out BSNOx emissions and gITE of LPDI and PFI in various fuel pressures and timings. Since the H_2 flow is always choked at this boost level, regardless of the injection strategy, it is only influenced by the fuel pressure and duration. Due to the effects of increased momentum and shorter injection duration to maintain constant BMEP (resulting in a longer mixing time), it is expected that overall mixture homogeneity improves at high fuel pressure for late LPDI, which reduces both fuel-rich and fuel lean local pockets, consequently, lowers NOx and unburnt H_2 emissions formation. This is particularly true for the case with SOI at −130 ^{o}CA, which has the shortest mixing time for H_2 and air. The BSNOx of late LPDI (SOI: 130 ^{o}CA) decreases from 3.08 g/kWh to 0.76 g/kWh as the fuel pressure increases from 12.8 bar to 20 bar. This remarkable 75 % NOx reduction indicates an optimum fuel pressure for late LPDI. As the SOI gradually advances from −130 to −150 ^{o}CA aTDC, the influence of fuel pressure becomes less dominant due to the increased mixing timing. Among the three injection strategies, PFI generally produces lower NOx emissions compared to late LPDI, despite a comparable global lambda value, highlighting the importance of mixture homogeneity to NOx

Table 1
Uncertainty of experimental apparatus.

Parameter	Principle	Uncertainty
NO/NO2/NOx	Heated_CLD	±(1 ppm or 2 % of reading), whichever is greater [35]
Unburnt H_2	Mass spectrometry	±2 % of reading [35]
Cylinder pressure	Piezoelectric	±1 % [36]
Crank angle	crank angle encoder	0.1°CA [36]
Fuel Mass flow	Corolis	±0.25 % [37]
Air mass flow	Corolis	±0.25 % [37]

Table 2
Operating matrix.

	PFI	Early LPDI	Late LPDI
BMEP [bar]	10 ± 0.2	10 ± 0.2	10 ± 0.2
Speed [rpm]	1000	1000	1000
CA50 [°CA aTDC]	~8	~8	~8
Pfuel [bar]	4–10	12–30	12–30
SOI [°CA aTDC]	−320	−260	−140/-130/-120
Spark [°CA aTDC]	Varies	Varies	Varies
EGR%	0	0	0
lambda	2.23	2.26	2.3
Boost (absolute) [bar]	1.99	2.07	1.77

formation. Early LPDI, however, results in even lower NO_x emissions than PFI. In this case, early LPDI benefits from both a relatively long time for mixing and stronger in-cylinder turbulence due to the higher fuel pressure of the DI injector. This results in an even more uniform mixture distribution, thereby suppressing local hot spots that favor NO_x formation [38]. Fig. 5b shows that both early and late LPDI reduce unburnt H_2 with increasing fuel pressure, consistent with the simultaneous decrease in BSNOx. This highlights the critical role of fuel pressure in LPDI H2ICE operation, as higher pressure enhances mixture homogeneity despite limited mixing time. As illustrated in Fig. 6a, PFI, and early LPDI exhibit comparable gITE, both achieving a peak value of approximately 41.6 %. In contrast, late LPDI demonstrates a modest increase in gITE as the SOI advances toward top dead center (TDC), reaching a maximum gITE of 41.9 %. The variations in gITE observed at different fuel rail pressures are attributed to minor shifts in combustion phasing (CA50), as shown in Fig. 3c. Overall, the three hydrogen injection strategies yield similar gITE performance, consistently exceeding 41 %. A slight efficiency advantage is observed for late LPDI; however, this gain remains within the estimated system uncertainty and should therefore be interpreted with caution.

When it comes to combustion stability, all three injection strategies successfully maintain COV_{nIMEP} below 1 % at 10 bar BMEP (Fig. 6b). Similarly, PRR (Fig. 6c) is also kept below 10 bar/°CA for all injection strategies. It is noteworthy that late LPDI shows higher PRR than early LPDI cases. This is most likely due to the increased mixture stratification in late LPDI, resulting in regions with a lower lambda and thus higher flame speed compared to early LPDI and PFI. This corroborates well with the shorter burn duration found for late LPDI as shown in Fig. 3. Additionally, the late LPDI presents narrower aROHR profiles (Fig. 7) and higher peak than PFI, indicating a faster burn rate. Despite the shortened injection duration at high fuel pressure, the overal cylinder pressure and heat release rate profiles remain quite similar regardless the fuel pressure.

6. Effects of injection strategy on high load

This section mainly focuses on the high operating load (BMEP:20 ± 1 bar) cases, where problematic combustion events like pre-ignition and knock occur more frequently. Three different H_2 injection strategies on SI H2ICE, namely: PFI, early LPDI, and late LPDI are compared and the effects of SOI will be discussed. To be more specific, the SOI of PFI is changed from −320 to −295 °CA, the SOI of early LPDI is varied from −260 to −200 °CA (open valve period), and the SOI of late LPDI is swept from −150 to −95 °CA (closed valve period). As is shown in Table 4, the speed is constant at 1000 rpm and BMEP varies from 19.1 bar to 20.7 depending on the specific injection strategy. Spark timing is selected to balance the prevention of pre-ignition with the maximization of gITE across the three injection strategies. In late LPDI scenarios, the boost pressure is deliberately limited to ensure that the ratio of fuel pressure to

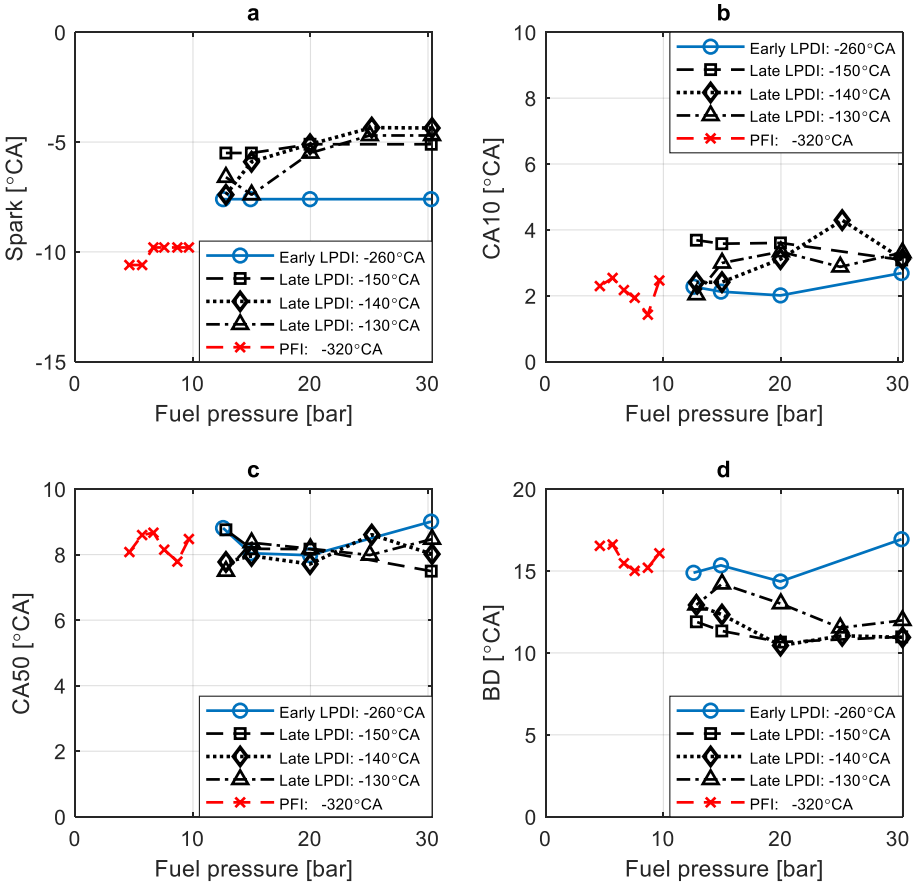

Fig. 3. Spark timing and combustion phasing at different fuel pressure for both PFI and LPDI.

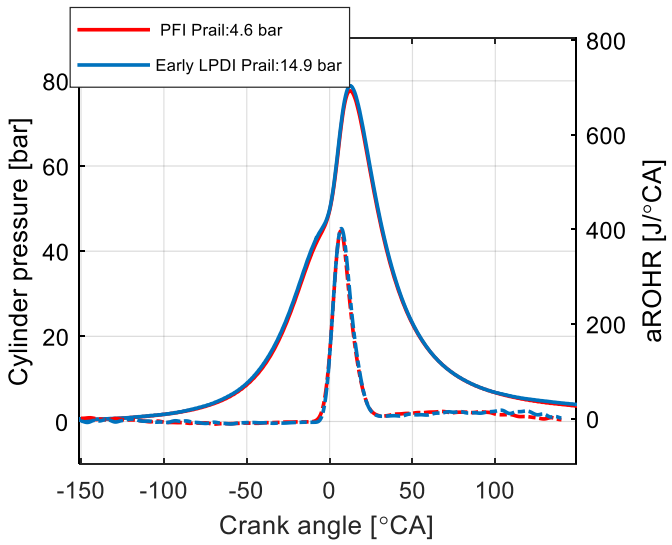

Fig. 4. Comparison of Cylinder pressure (left y axis) and aROHR (right y axis) for PFI and LPDI at same CA50.

Table 3
Key performance comparison between PFI and LPDI.

Parameters	PFI	Early LPDI
CA50 [°CA aTDC]	8.4	8.8
Burn duration [°CA]	16.5	15.3
gITE [%]	41.5 ± 0.8	41 ± 0.8
PRR [bar/°CA]	6.3	6.3

cylinder pressure at the end of injection ratio does not exceed 1.9, thereby maintaining sonic flow conditions. Since the boost pressure directly contributes to the cylinder pressure (i.e. < 21 bar) at the end of injection. Moreover, the late LPDI benefits from the enhanced volumetric efficiency, as the injection commences after intake valve closes. On the contrary, the early LPDI likely presents a similar level of volumetric efficiency as PFI since injection happens during inlet valve open period. Therefore, late LPDI is operated at 3.11 bar boost pressure (lambda 2.23), Early LPDI is operated at 3.76 bar (lambda 2.31), and PFI is operated at 3.83 bar (lambda 2.14). Table 5 gives an better understanding of volumetric efficiency (air mass flow) for three injection strategies at identical operating points. It is shown that the inlet air flow for PFI (Boost: 3.84 bar, Air flow: 232.9 kg/h) and LPDI (Boost: 3.76 bar Airflow: 228.2 kg/h) are essentially identical with same boost level, while late LPDI presents 5.6 % higher air flow with 11.3 % lower boost pressure than these two open valve injection strategies.

It is shown in Fig. 8 that the CA10, CA50, and CA90 stay relatively constant, and similarly, CA10 and CA50 for early LPDI for different SOI timings. However, in the case of SOI = −250 °CA aTDC, both CA10 and CA50 occur earlier due to pre-ignition as is illustrated in Fig. 9a. Early LPDI at −250 shows heat release before spark timing. Moreover, this LPDI strategy shows advanced CA90 and consequently shorter burn duration as injection timing shifts from −240 to −200 °CA aTDC. This higher heat release rate is also illustrated by the higher peak of the aROHR curves in Fig. 9a. For late LPDI cases, CA10 and CA50 show an initial plateau from −150 to −130 °CA aTDC, followed by an advancing trend as SOI is further delayed to −90 °CA aTDC. Despite this early rapid combustion, CA90 fluctuates between SOI -125 to −95 °CA cases. This behavior is explained by the aROHR curves in Fig. 9b and c, which exhibit a transition of combustion regimes. The rate of heat release remains relatively stable from SOI -150 to −130 °CA, after which combustion initiates more rapidly. This is attributed to the increased mixture stratification for an SOI beyond −125 °CA, leading to co-existence of both locally fuel-rich and lean regions within the combustion chamber. The high-equivalence ratio zones ignite and propagate more rapidly in the early combustion stages compared to earlier LPDI injection timings. Similar results are also found in a simulation work [39] where delayed H2 direct injection timing exhibits more rapid flame speed and higher peak cylinder pressure due to increased mixture heterogeneity and stratification. However, the regions with a lower equivalence ratio exhibit a slower burnout. These combined effects contribute to the observed fluctuation in burn duration for late LPDI between SOI -125 and −95 °CA.

Fig. 10 shows that PFI achieves a gross indicated thermal efficiency (gITE) of up to 41 %, with only minor sensitivity to injection timing. Early LPDI provides a slight improvement, reaching a gITE up to 41.7 %. Among the three injection strategies, late LPDI exhibits the lowest heat transfer loss (Fig. 11), which directly contributes to its superior efficiency. As is shown in Fig. 11, late LPDI presents a heat loss in the range of 10.4–12.9 %, while that of early LPDI and PFI are in the range of 13.1–15.7 % and 13.3–15.6 % respectively. In this analysis, heat transfer loss is defined as the difference between the total energy content of the injected fuel (based on lower heating value) and the maximum of apparent heat release. Combustion loss is computed from the unburnt H_2 measured in the exhaust. Exhaust loss is determined from the remaining fraction of the total energy input. Notably, gITE in the late LPDI case increases progressively as SOI is delayed. This improvement is attributed to a reduction in compression work at later injection timings, as illustrated in Fig. 12. A peak gITE of approximately 42.4 % was achieved at an SOI of −95 °CA aTDC. Compared with the other strategies, late LPDI delivers efficiency gains of 0.7 percentage points over early LPDI and 1.4 percentage points over PFI. Although the measurement uncertainty is estimated at ±0.4 %, the trend consistently indicates that late LPDI

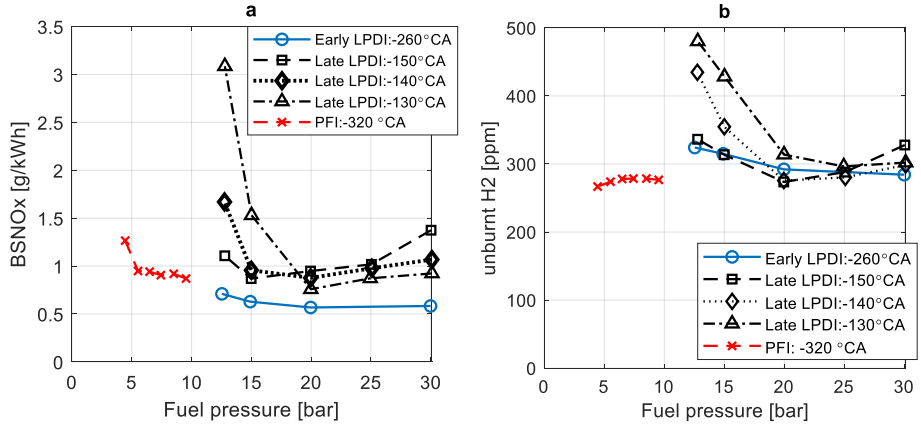

Fig. 5. Engine-out BSNOx emissions and unburnt H2 at various fuel pressure.

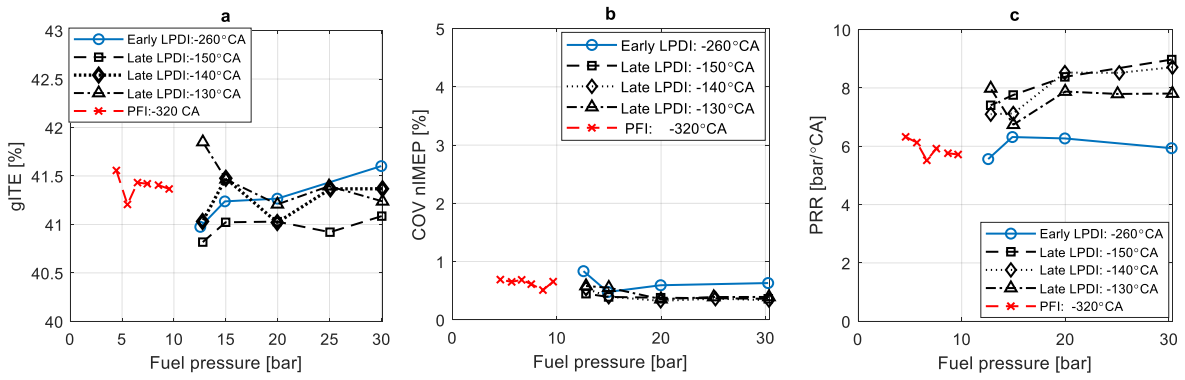

Fig. 6. Gross indicated efficiency(a), pressure rise rate (b) and COV of nIMEP (c) at various fuel pressure and injection timing.

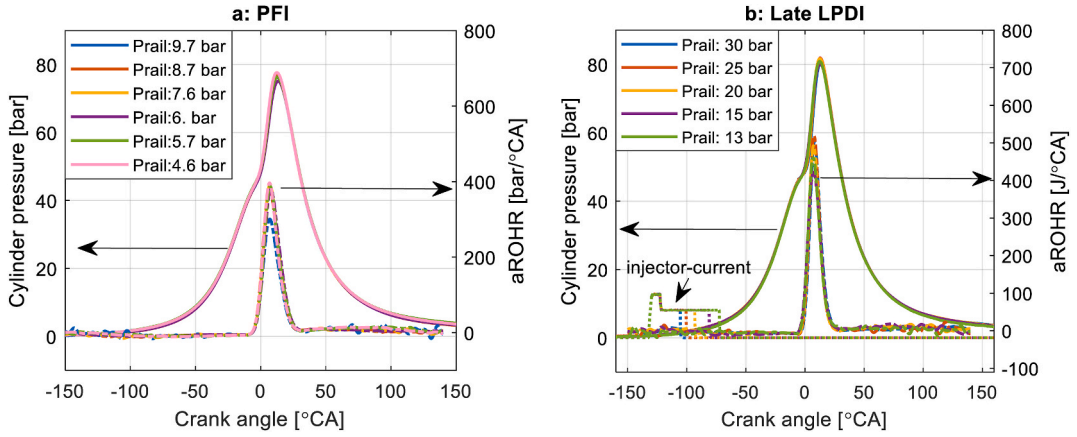

Fig. 7. Cylinder pressure and aROHR from different fuel pressure for PFI (a) and late LPDI (b).

Table 4
Operating matrix.

	PFI	Early LPDI	Late LPDI
BMEP [bar]	20.7 ± 0.2	19.7 ± 0.2	19.1 ± 0.2
Speed [rpm]	1000	1000	1000
SOI [°CA aTDC]	varied	varied	varied
Absolute Boost [bar]	3.84	3.76	3.11
P fuel [bar]	7	40	40
Lambda [−]	2.14 ± 0.01	2.31 ± 0.01	2.23 ± 0.01
Spark [°CA aTDC]	−4	−3.8	−2.7

Table 5
Comparison of three injection strategies at similar operating points.

	PFI	Early LPDI	Late LPDI
BMEP [bar]	20.7 ± 0.4	20.9 ± 0.4	20.7 ± 0.4
Speed [rpm]	1000	1000	1000
SOI [°CA aTDC]	−320	−260	−150
Boost [bar]	3.84	3.81	3.38
P fuel [bar]	7	30	30
Lambda [−]	2.13 ± 0.01	2.12 ± 0.01	2.24 ± 0.01
Spark [°CA aTDC]	−4	−5.9	−5.9
gITE [%]	40.8	41.88	41.15
BSNOx [g/kWh]	2.64	3.33	3.78
H2 [ppm]	181	148	105
PRR[bar/°CA]	6.7	6.9	9.2
Qair [kg/h]	232.9	228.2	240.9
COVIMEP [%]	0.79	0.54	0.512
PI ratio [%]	3	0	1
CA50 [°CA aTDC]	12.8	11.5	10.1

offers the greatest potential for achieving higher thermal efficiency in H_2-fueled engines. This increased efficiency H_2ICE performance of late LPDI is also reported in simulation work [40] that ITE increases remarkably as injection timing delays from −190 to −100 °CA aTDC, reaching a peak ITE of 40.5 %. This enhancement is attributed to the inhibition effect of gas mixture delamination on wall heat loss [41].

Although all three injection strategies show low COV_{nIMEP} irrespective of injection timing. The late LPDI shows much higher PRR (up to 19.7 bar/°CA at injection timing of −95 °CA aTDC) than PFI and early LPDI and it increases as LPDI timing gets close to TDC. This is directly related to the mixture stratification. Compared to early LPDI and PFI, the largely reduced mixing time seems to be more influential at a retarded SOI and contributes to a more stratified mixture. The presence of locally richer H_2/air pockets apparently lead to these high PRR. This is further supported by the fact that late LPDI produces more BSNOx (from the richer regions) and unburnt H_2 emissions (from the leaner regions). The range of equivalence ratios obviously increases at later LPDI injection timings. It should be noted, however, that all three injection strategies retain a low PI ratio mostly below 3 %. At −250 °CA aTDC, an early LPDI case exhibited a pre-ignition (PI) occurrence ratio of up to 6 %. The cylinder pressure and aROHR traces of these pre-ignition cycles, shown in Figure 14 in Appendix, reveal a noticeable heat release and pressure rise occurring prior to the spark timing.

In terms of engine-out emissions, early LPDI generates the least BSNOx emissions among the three injection strategies (Fig. 13). Firstly, the early injection timing leaves enough mixing time for H_2 and air, resulting in largely well-mixed mixtures. Secondly, early LPDI cases were performed with the highest lambda (i.e. 2.31), causing lowest bulk temperature. These two combined factors bring about an engine-out BSNOx emissions as low as 0.72 g/kWh. On the contrary, late LPDI

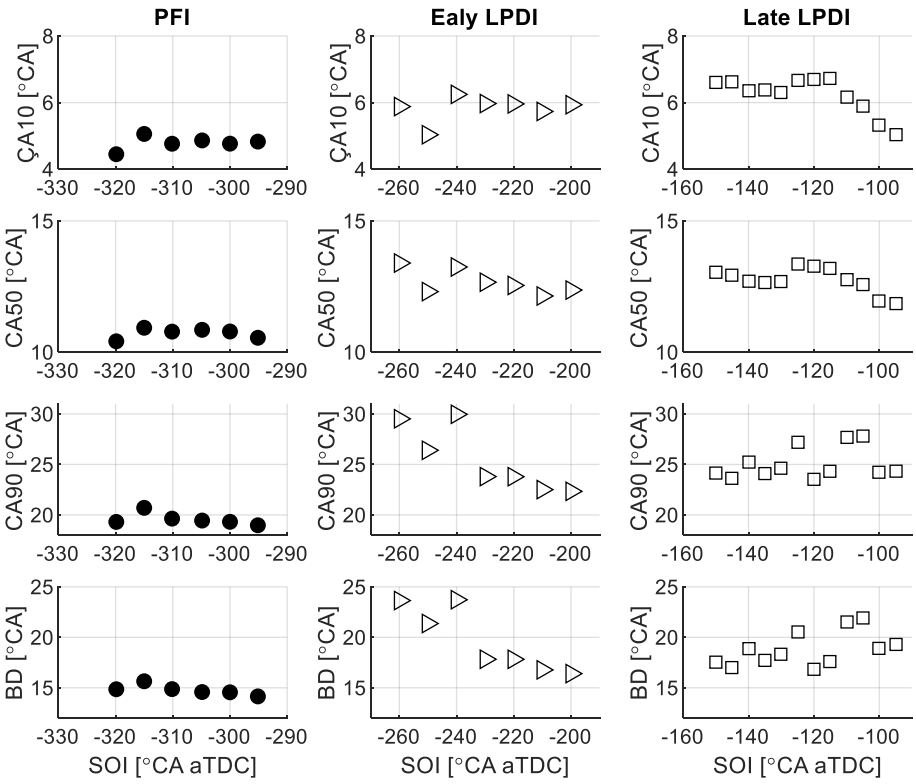

Fig. 8. Combustion phasing for PFI and LPDI at different injection timing.

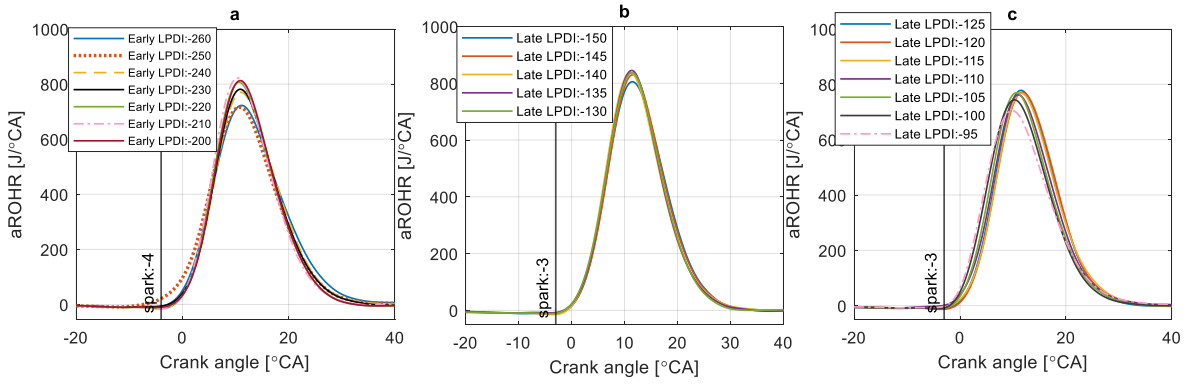

Fig. 9. aROHR profiles of various LPDI injection timings.(a, DI: 260 to −200 °CA aTDC b, DI: 150 to −130 °CA aTDC, c DI: 125 to −95 °CA aTDC).

produces the highest BSNOx and unburnt H_2 emissions. Both increase with the injection timing delays, as expected, due to increased charge stratification at a late SOI. Up to 9.3 g/kWh of BSNOx and 435 ppm unburnt H_2 are observed at an SOI of −95 °CA.

To provide a direct comparison among the three injection strategies, Table 5 summarizes the key performance indicators at identical operating conditions. Combined r with the findings from the injection timing sweep, it can be inferred that, the gITE is strongly influenced by CA50 and overall lambda. Both the PFI and early LPDI (inject in the open valve period) exhibit similar intake air mass, suggesting comparable volumetric efficiency regardless of the specific injection location within the valve open period. When injection timing is sufficiently early, the resulting mixture homogeneity is also expected to be similar. In contrast, late LPDI (injection during the intake valve closed period) shows a clear benefit in improving gITE, primarily due to reduced compression work. However, this improvement comes at the expense of increased engine-out NOx and unburned H_2 emissions, which are attributed to greater mixture stratification and reduced homogeneity.

7. Summary and conclusions

This study directly compares PFI and LPDI systems on the same single-cylinder H_2 HD engine, aiming to develop next-generation heavy-duty H_2ICE targeting future Euro 7 HD truck application. Three injection strategies are specifically investigated: PFI, early LPDI (SOI between −300° and −200°CA, before intake valve closes), and late LPDI (SOI between −150° and −90°CA, after intake valve closes). The experimental parameter study examines variations in fuel pressure and injection timing, exploring the trade-offs between efficiency and emissions to fully harness hydrogen's potential as a sustainable fuel. The single-cylinder engine tests were performed both on medium load (BMEP: 10 bar) and high load (BMEP>19 bar). Based on the results and discussions, the following conclusions were drawn.

1. At 10 bar BMEP, early LPDI benefits from a long mixing time and shows similar heat release profiles as PFI at a specific phasing. This also leads to similar gross indicated thermal efficiency (maximum

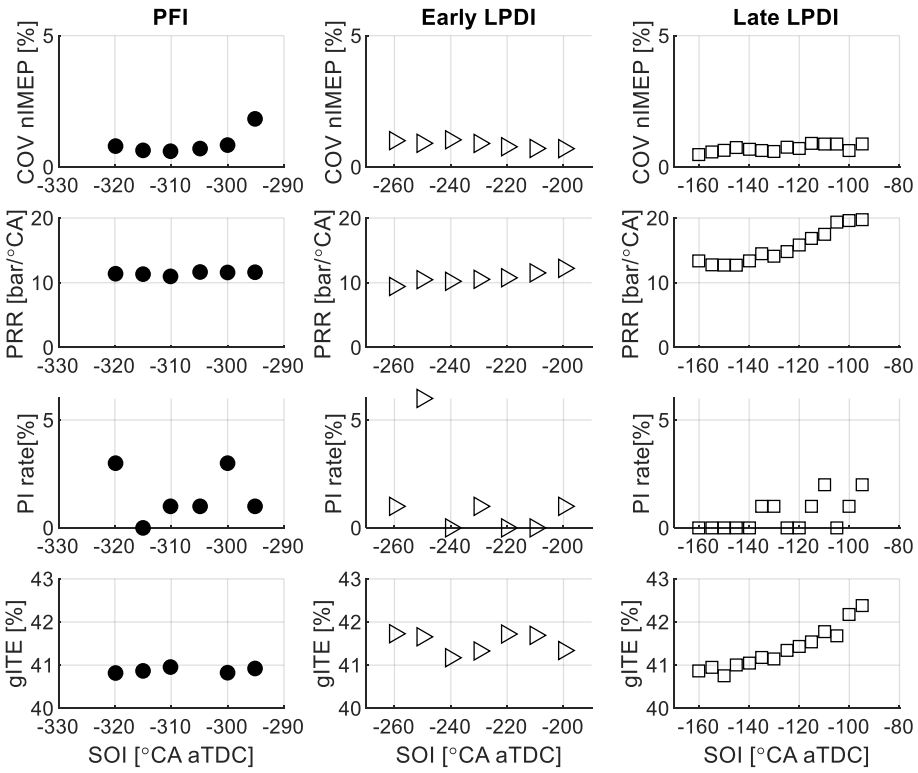

Fig. 10. Key performance parameters for PFI and LPDI at different injection timing.

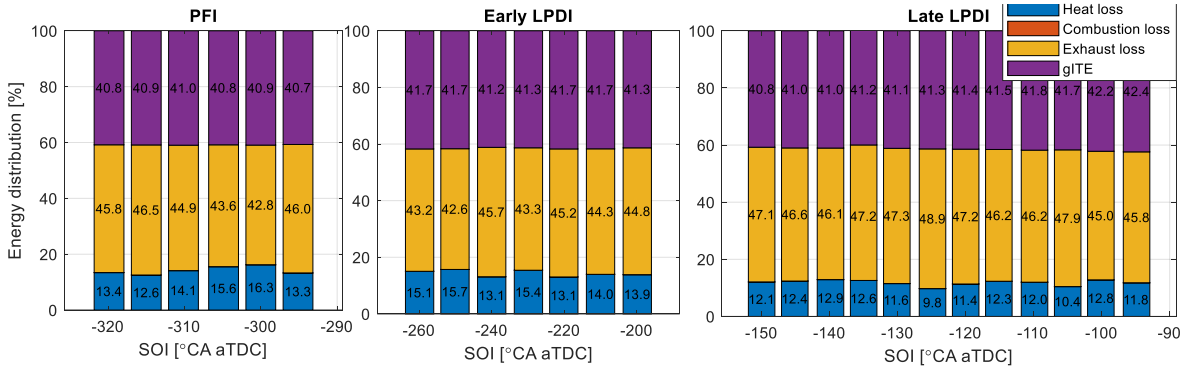

Fig. 11. Energy distribution analysis of PFI, early LPDI, late LPDI injection strategies.

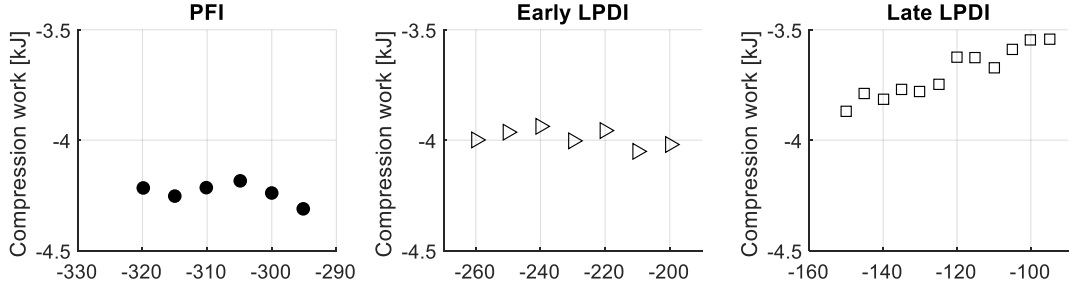

Fig. 12. Compression work of different injection strategies.

41.6 %), stability (PRR and COV_{nIMEP}). Late LPDI suffers from decreased mixing time, making the H_2/air mixture less homogeneous and more stratified compared to PFI and early LPDI. Therefore it presents higher PRR and NOx emissions. Up to 41.9 % gITE was achieved at the late LPDI (−130 °CA aTDC).

2. At 10 bar BMEP, NOx emissions in general are sensitive to lambda and combustion phasing. Although with similar level of mixture homogeneity, early LPDI benefits from long mixing time and effects of higher fuel pressure, and therefore produces the least engine-out NOx emissions (0.57 g/kWh). Late LPDI shows the highest engine-

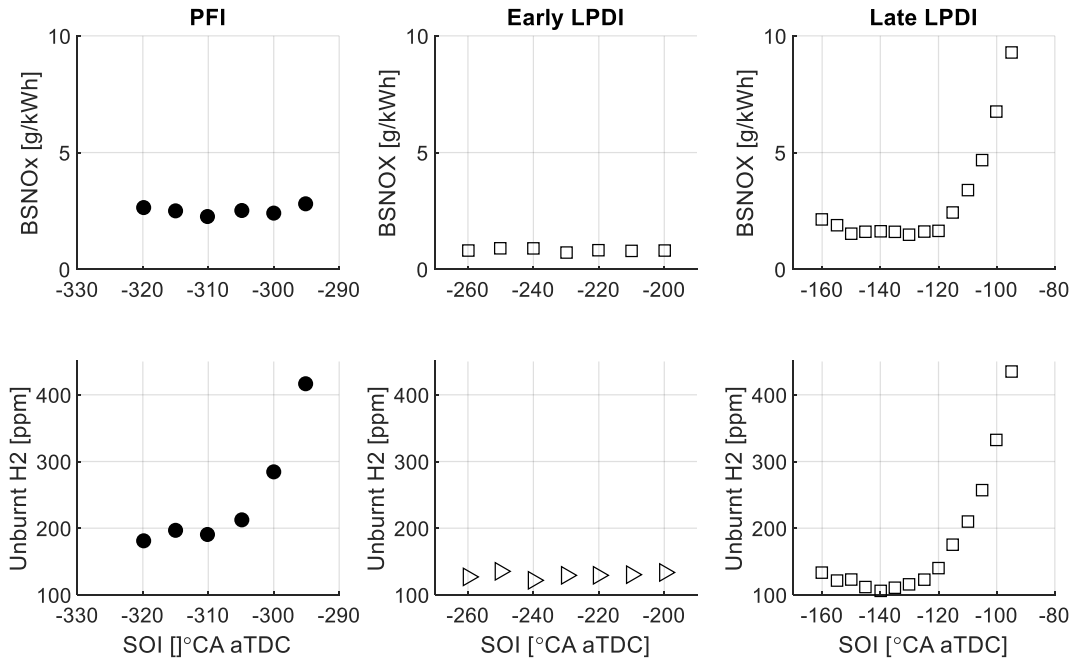

Fig. 13. Engine-out NOx and unburnt H2 at different injection timing.

out BSNOx emission and a high fuel pressure is crucial to improve mixture homogeneity of late LPDI, therefore significantly less engine-out NOx emissions production. Up to 75 % reduction of BSNOx is achieved by increasing fuel pressure from 12.8 to 20 bar.

3. As the load increases to above 19 bar BMEP, combustion phasing is not significantly affected by variations in injection timing. All three injection strategies achieve 41 % gITE. Moreover, late LPDI achieves the highest gITE due to reduced heat transfer losses, with efficiency increasing as SOI approaches TDC as a result of lower compression work. A peak gITE of 42.4 % is observed at an SOI of −95°CA aTDC. Notably, the identical air mass flow of PFI and early LPDI under the same operating conditions indicates comparable volumetric efficiency.
4. At high load condition, all three injection strategies show good combustion stability (low COV_{IMEP} and acceptable PRR). Furthermore, the pre-ignition rate is kept within 6 % regardless the injection method and injection timing. Although late LPDI is constrained by boost pressure, it achieves higher volumetric efficiency than both PFI and early LPDI. The late LPDI suffers from the short mixing time and unevenly distributed rich hydrogen/air pockets, leading to increased engine-out BSNOx (up to 9.3 g/kWh), unburnt H_2 (up to 435 ppm), and PRR (up to 19.7 bar/^{o}CA). Yet, late LPDI presents the highest potential of gITE gain among three injection strategies.

In summary, this study demonstrates how injection strategies, injection timing, and fuel pressure shape the performance of a single-cylinder heavy-duty H2ICE. The low-pressure direct injection (LPDI) strategy provides flexibility to balance efficiency and emissions. Early LPDI, with its premixed charge formation, is highly effective at reducing NOx—particularly at low and medium loads. In contrast, late LPDI leverages charge stratification at high loads, achieving superior thermal efficiency. Together, these findings highlight LPDI as a versatile fueling strategy for hydrogen engines, offering both substantial NO_x reduction and efficiency gains depending on operating conditions.

CRediT authorship contribution statement

Jinlin Han: Writing – original draft, Visualization, Investigation, Formal analysis, Data curation. **Erik Doosje:** Writing – review & editing, Validation, Formal analysis, Conceptualization. **Xander Seykens:** Writing – review & editing, Project administration, Funding acquisition, Formal analysis. **L.M.T. Somers:** Writing – review & editing, Resources, Funding acquisition, Formal analysis.

Declaration of competing interest

The authors declare that they have no known competing financial interests or personal relationships that could have appeared to influence the work reported in this paper.

Acknowledgement

This work is funded by the Top sector HTSM Automotive program of the Dutch Ministry of Economic Affairs and Climate Policy, as part of the project “Green Transport Delta – Hydrogen”, in collaboration with industry partners.

Appendix

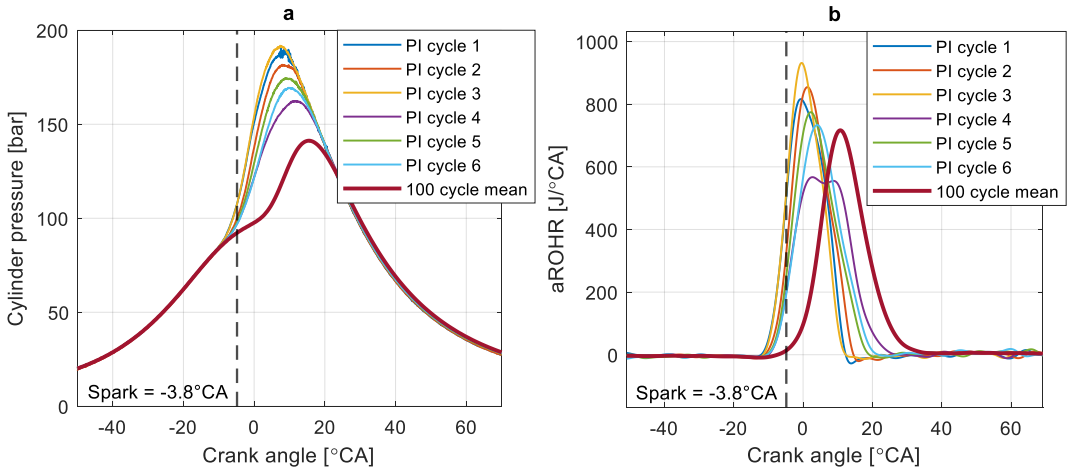

Fig. A1. Cylinder pressure (a) and aROHR (b) of early LPDI (SOI: 250 °CA aTDC) with pre-ignition.

References

[1] Regulation - 2021/1119 - EN - EUR-LEX. (n.d.). http://data.europa.eu/eli/reg/2021/1119/oj.

[2] Cells F. Hydrogen 2 Joint Undertaking, Hydrogen roadmap Europe: a sustainable pathway for the European energy transition. Publications Office; 2019.

[3] Road transport: Reducing CO_2 emissions from vehicles. (n.d.). Climate Action https://climate.ec.europa.eu/eu-action/transport/road-transport-reducing-co2-emissions-vehicles_en.

[4] Irles S. Europe sets the bar high and approves a 90% CO2 emission reduction target in new trucks by 2040 - International Council on Clean Transportation. International Council on Clean Transportation 2024. https://theicct.org/europe-sets-the-bar-high-and-approves-a-90-co2-emission-reduction-target-in-new-trucks-by-2040/.

[5] Editor Engineeringtoolbox. Higher calorific values of common fuels: Reference & data. https://www.engineeringtoolbox.com/fuels-higher-calorific-values-d_169.html; 2025.

[6] Suwaileh W, Bicer Y, Al Hail S, Farooq S, Yunus RM, Rosman NN, Karajagi I. Exploring hydrogen fuel as a sustainable solution for zero-emission aviation: Production, storage, and engine adaptation challenges. Int J Hydrogen Energy 2025;121:304–25.

[7] Han J, Somers LMT. Low-temperature combustion analysis of butanol isomer/diesel blends under reduced oxygen conditions in a constant volume combustion chamber. Case Stud Therm Eng 2025;68.

[8] Gao J, Wang X, Song P, Tian G, Ma C. Review of the backfire occurrences and control strategies for port hydrogen injection internal combustion engines. Fuel 2022;307:121553.

[9] Khalid AH, Said MFM, Veza I, Abas MA, Roslan MF, Abubakar S, Jalal MR. Hydrogen port fuel injection: review of fuel injection control strategies to mitigate backfire in internal combustion engine fuelled with hydrogen. Int J Hydrogen Energy 2024;66:571–81.

[10] Turner JW. Future technological directions for hydrogen internal combustion engines in transport applications. Applications in Energy and Combustion Science 2025;21:100302.

[11] Ning D, Dong J, Guan W, Wang Z, Wang H, Lin T, Pan M. Experimental analysis and multi-objective optimization of heavy-duty hydrogen SI engine performance and emissions based on GA-BP-MOGWO. Energy Convers Manag 2025;329:119638.

[12] Oktar HE, Tonyali IH, Apaydin AH. A cost-effective and sustainable path to a green future: retrofitting internal combustion engines for hydrogen fuel utilization. Int J Hydrogen Energy 2025;143:969–77.

[13] Bekdemir C, Doosje E, Seykens X. H2-ICE technology options of the present and the near future. SAE Technical Paper 2022-01-0472 2022. https://doi.org/10.4271/2022-01-0472.

[14] Willems R, Seykens X, Bekdemir C, Doosje E, Van Gompel P. The potential of hydrogen high pressure direct injection toward future emissions compliance: optimizing engine-out NOx and thermal efficiency (No. 2024-37-0005). SAE technical paper. 2024.

[15] Seykens X, Doosje E, Bekdemir C, van Gompel P. Hydrogen combustion concepts: comparison of port fuel injection with spark ignition and high pressure direct injection (HPDI™)–Power density, efficiency and emissions. In: 44th international l Vienna motor symposium; 2023.

[16] França LBM, Pasa BR, Fagundez JLS, Pereira JS, Martins MES, Lanzanova TDM, Salau NPG. Validation of a CFD hydrogen combustion model on an PFI SI engine under lean combustion (No. 2023-36-0125). SAE Technical Paper 2024.

[17] Bao LZ, Sun BG, Luo QH, Li JC, Qian DC, Ma HY, Guo YJ. Development of a turbocharged direct-injection hydrogen engine to achieve clean, efficient, and high-power performance. Fuel 2022;324:124713.

[18] Zhang SW, Sun BG, Lin SL, Li Q, Wu X, Hu T, Luo QH. Energy and exergy analysis for a turbocharged direct-injection hydrogen engine to achieve efficient and high-economy performances. Int J Hydrogen Energy 2024;54:601–12.

[19] Lai FY, Sun BG, Xiao G, Luo QH, Bao LZ. Research on optimizing turbo-matching of a large-displacement PFI hydrogen engine to achieve high-power performance. Int J Hydrogen Energy 2023;48(97):38508–20.

[20] Kim J, Rajoo S. A numerical study on turbocharging system for PFI-SI type hydrogen combustion engine. SAE technical paper 2021-24-0094. 2021. https://doi.org/10.4271/2021-24-0094.

[21] Frigo S, Bonini D, De Regibus S, Sguaitamatti L. Experimental analysis of boost limits in a hydrogen fueled PFI internal combustion engine. J Phys Conf 2023, December;2648(1):012073. IOP Publishing.

[22] Mohamed M, et al. Hydrogen engine insights: a comprehensive experimental examination of port fuel injection and direct injection. SAE technical paper 2024-01-2611. 2024. p. 1–16. https://doi.org/10.4271/2024-01-2611.

[23] Silveira JP, Fagundez JLS, Garlet RA, Martins MES, Salau NPG, Lanzanova TDM. Hydrogen-fueled PFI SI engine investigation for near-zero NOx emissions in de-throttled and supercharged ultra-lean burn conditions. Int J Hydrogen Energy 2024;91:800–13.

[24] Wang Z, Chen Y, Li Q, Tang X, Yang Z, Wang D, Diya A. Impact of hydrogen-injected parameters on the stratified air-fuel mixture formation and combustion of the direct injection hydrogen engine. Energy Convers Manag 2024;321:119083.

[25] Lee S, Kim G, Bae C. Effect of mixture formation mode on the combustion and emission characteristics in a hydrogen direct-injection engine under different load conditions. Appl Therm Eng 2022;209:118276.

[26] Molina S, Novella R, Gomez-Soriano J, Olcina-Girona M. Impact of medium-pressure direct injection in a spark-ignition engine fueled by hydrogen. Fuel 2024;360:130618.

[27] Thawko A, Eyal A, Tartakovsky L. Experimental comparison of performance and emissions of a direct-injection engine fed with alternative gaseous fuels. Energy Convers Manag 2022;251:114988.

[28] Maio G, Boberic A, Giarracca L, Aubagnac-Karkar D, Colin O, Duffour F, Pischinger S. Experimental and numerical investigation of a direct injection spark ignition hydrogen engine for heavy-duty applications. Int J Hydrogen Energy 2022;47(67):29069–84.

[29] Gammaidoni T, Miliozzi A, Zembi J, Battistoni M. Hydrogen mixing and combustion in an SI internal combustion engine: CFD evaluation of premixed and DI strategies. Case Stud Therm Eng 2024;55:104072.

[30] Pasa BR, Fagundez JLS, Martins MES, Salau NPG, Cogo VV, Prante GAF, Wittek K. Numerical analysis of the influence of SOI and injection duration on the homogenization of hydrogen-air mixtures in a PFI SI engine under lean operation (No. 2023-36-0106). SAE Technical Paper 2024.

[31] Musy F, Ortiz R, Ortiz I, Ortiz A. Hydrogen-fuelled internal combustion engines: direct injection versus port-fuel injection. Int J Hydrogen Energy 2024.

[32] Wang X, Sun BG, Luo QH, Bao LZ, Su JY, Liu J, Li XC. Visualization research on hydrogen jet characteristics of an outward-opening injector for direct injection hydrogen engines. Fuel 2020;280:118710.

[33] Verhelst S, Wallner T. Hydrogen-fueled internal combustion engines. Prog Energy Combust Sci 2009;35(6):490–527.

[34] Yeganeh M, Rönn K, Karimkashi S, Cheng Q, Hlaing P, Hyvönen J, Larmi M. Experimental investigations of hydrogen pre-ignition phenomenon induced by two different lubricating oils in a rapid compression expansion machine. Proc Combust Inst 2024;40(1–4):105715.
[35] https://static.horiba.com/fileadmin/Horiba/Products/Automotive/Emission_Measurement_Systems/MEXA-ONE/AUTOMOTIVE_EMISSION_ANALYZER_MEXA-ONE_EMISSION_MEASUREMENT_SYSTEMS_BROCHURE_EN.pdf.
[36] Han J, Bao H, Somers LMT. Experimental investigation of reactivity controlled compression ignition with n-butanol/n-heptane in a heavy-duty diesel engine. Appl Energy 2021;282:116164.
[37] https://www.emerson.com/documents/automation/article-direct-approach-to-mass-flow-measurement-micro-motion-en-64236.pdf.
[38] Hu Z, Yuan S, Wei H, Huang Z, Wei H, Chan SH, Zhou L. High-pressure injection or low-pressure injection for a direct injection hydrogen engine? Int J Hydrogen Energy 2024;59:383–9.
[39] Lou D, Rao X, Zhang Y, Fang L, Tan P, Hu Z. Investigation of impacts of hydrogen injection and spark strategy on knock in hydrogen engine. Int J Hydrogen Energy 2024;82:1252–62.
[40] Lu C, Chen W, Zuo Q, Kou C, Wang H, Xiao G, Ma Y. Numerical investigation on gaseous fuel injection strategies on combustion characteristics and NO emission performance in a pure hydrogen engine. Fuel 2024;363:130911.
[41] Wallner T, Matthias NS, Scarcelli R. Influence of injection strategy in a high-efficiency hydrogen direct injection engine. SAE International Journal of Fuels and Lubricants 2012;5(1):289–300.